© Pol J Radiol 2026; 91: e115-e123
DOI: https://doi.org/10.5114/pjr/215538

Received: 14.10.2025
Accepted: 12.12.2025
Published: 05.03.2026

Polish Journal of Radiology
http://www.polradiol.com

Original paper

CT-based texture analysis for preoperative prediction of key histopathological features in laryngeal cancer

Ahmet Bozer[1,A,C,D,E,F], Fatma Ceren Sarioglu[2,A,C,D,F], İlker Burak Arslan[3,A,B,C,D], Ulku Kucuk[4,B,C,F], Yeliz Pekçevik[1,D,E,F,G]

[1]Department of Radiology, Ministry of Health Izmir City Hospital, Izmir, Turkey
[2]Department of Radiology, Division of Paediatric Radiology, Dokuz Eylul University School of Medicine, Izmir, Turkey
[3]Department of Otolaryngology – Head and Neck Surgery, Ministry of Health Izmir City Hospital, Izmir, Turkey
[4]Department of Pathology, Ministry of Health Izmir City Hospital, Izmir, Turkey

Abstract

Purpose: Laryngeal squamous cell carcinoma (LSCC) is a malignancy with significant morbidity and mortality. Accurate preoperative assessment of key histopathological features, including lymph node metastasis (LNM), extranodal extension (ENE), lymphovascular invasion (LVI), perineural invasion (PNI), and thyroid cartilage invasion (TCI), is crucial for optimising treatment strategies. Computed tomography (CT)-based texture analysis, a radiomics approach, has shown potential in identifying tumour heterogeneity and aggressive histopathological behaviour. The aim of the study was to evaluate the predictive value of CT-based texture analysis for detecting key histopathological features in LSCC and assess its potential as a non-invasive tool for preoperative risk stratification.

Material and methods: This retrospective study included 32 LSCC patients who underwent contrast-enhanced neck CT within 4 weeks before surgery. Texture features were extracted using LIFEx software. Mann-Whitney *U* tests and receiver operating characteristic (ROC) curve analyses were performed to assess diagnostic performance.

Results: Significant texture features were identified for LNM, ENE, and TCI ($p < 0.05$). GLZLM_HGZE ≤ 4635 predicted LNM with an AUC of 0.847 (95% CI: 0.708-0.986), sensitivity of 71%, and specificity of 84%. For ENE, GLZLM_HGZE ≤ 4625 achieved an AUC of 0.891, sensitivity of 85%, and specificity of 84%. TCI prediction was highest with GLZLM_SZLGE ≥ 0.00118 (AUC: 0.964, 95% CI: 0.909-1.000), with sensitivity of 88% and specificity of 93%. No significant predictors were found for LVI or PNI.

Conclusions: CT-based texture analysis is a promising non-invasive tool for preoperative risk assessment in LSCC, particularly for LNM, ENE, and TCI. Further validation in larger studies is warranted.

Key words: laryngeal squamous cell carcinoma, CT-based texture analysis, radiomics, lymph node metastasis, extranodal extension.

Introduction

Laryngeal squamous cell carcinoma (LSCC) is a significant global health concern, with approximately 184,615 new cases and 99,840 deaths reported in 2020 (age-standardised rate [ASR]: 2.0 and 1.0 per 100,000, respectively) [1]. Incidence and mortality rates vary geographically, being highest in the Caribbean (ASR = 4.0) and Eastern Europe (ASR = 3.6), with men having a sevenfold higher risk than women [1]. Over the past 3 decades, the incidence of LSCC has risen, while mortality has declined slightly, probably due to reduced tobacco and alcohol use and advancements in diagnostic and treatment strategies.

In LSCC, in addition to well-established prognostic factors such as clinical (TNM classification, age, smok-

Correspondence address:
Ahmet Bozer, Department of Radiology, Ministry of Health Izmir City Hospital, 2148/11 St., 35540 Izmir, Turkey, e-mail: drahmetbozer@gmail.com

Authors' contribution:
A Study design · **B** Data collection · **C** Statistical analysis · **D** Data interpretation · **E** Manuscript preparation · **F** Literature search · **G** Funds collection

ing), molecular (HPV association, TP53 mutations), and treatment-related factors (organ preservation vs. surgery, surgical margins, response to treatment), pathological features – including lymph node metastasis (LNM), extranodal extension (ENE), lymphovascular invasion (LVI), and thyroid cartilage invasion (TCI) – also play a crucial role [2-6]. Accurate preoperative assessment of these characteristics is essential for determining optimal surgical and therapeutic strategies. Conventional imaging modalities such as computed tomography (CT) are fundamental for cancer staging but may be limited in detecting subtle microstructural changes indicative of aggressive histopathological behaviour.

CT-based texture analysis enables preoperative prediction of histopathological features, optimising surgical planning and treatment strategies [7-9]. This approach provides non-invasive predictive insights, facilitating the determination of surgical extent, guiding the need for adjuvant therapy, and improving prognostic assessment while reducing unnecessary interventions.

Over the past decade, advanced analytical techniques, including texture analysis and radiomics, have gained increasing attention in radiology research [10]. Texture analysis, a radiomics-based approach, quantifies tumour heterogeneity by evaluating pixel intensity distributions within imaging data. This method has shown promise in improving diagnostic accuracy, prognostic assessment, and treatment response evaluation across various malignancies [11-13]. However, studies investigating texture-based models for predicting key histopathological features in LSCC remain limited.

Recent studies suggest that CT-derived radiomic features may aid in predicting the histopathological characteristics of LSCC. Guo *et al.* [14] analysed contrast-enhanced CT images from 265 LSCC patients and demonstrated the potential of machine learning-assisted radiomic models for detecting thyroid cartilage invasion, achieving superior diagnostic accuracy compared to radiologists. These findings support the growing role of radiomics as a non-invasive tool in oncologic imaging.

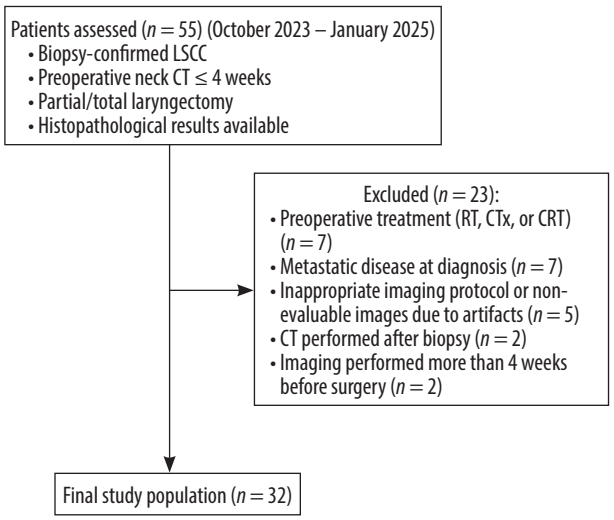

LSCC – laryngeal squamous cell carcinoma, CT – computed tomography, CTx – chemotherapy, RT – radiotherapy, CRT – concurrent chemoradiotherapy

Figure 1. Flowchart depicting the patient selection process

Radiomics has also been explored for survival prediction in LSCC. Rajgor *et al.* [15] identified specific radiomic features, such as shape compactness and grey-level zone length matrix non-uniformity, as independent prognostic biomarkers in advanced LSCC. Elevated values of these features correlated with poorer 5-year disease-specific survival, suggesting their potential role in refining treatment strategies. These findings underscore the clinical utility of advanced imaging analyses in improving the diagnostic and prognostic evaluation of LSCC.

This study aims to evaluate the predictive value of CT-based texture analysis for identifying key histopathological features in LSCC, including LNM, ENE, perineural invasion (PNI), LVI, and TCI. By analysing radiomic features extracted from contrast-enhanced CT images, we seek to develop a non-invasive preoperative assessment tool that may enhance clinical decision-making and improve patient stratification for treatment planning.

Material and methods

Patient selection

This study was initiated after obtaining approval from the institutional Ethics Committee (Ethics Committee Approval: Decision No. 2024/247, Date 08.01.2025).

Between October 2023 and January 2025, patients diagnosed with LSCC via biopsy, who underwent preoperative neck CT within 4 weeks before surgery, underwent partial or total laryngectomy, and had available histopathological results, were included.

Exclusion criteria included:

- Patients who received preoperative treatment (radiotherapy [RT], chemotherapy [CTx], or concurrent chemoradiotherapy [CRT]) (n = 7),
- Patients with metastatic disease at diagnosis (n = 7),
- Patients with imaging performed with an inappropriate protocol or images non-evaluable due to artifacts (n = 5),
- Patients who underwent CT after biopsy (n = 2),
- Patients with imaging performed more than 4 weeks before surgery (n = 2).

A total of 32 patients were included in the study (Figure 1).

CT imaging protocol

All CT scans were performed using a 256-detector CT scanner (GE Revolution EVO, GE Healthcare, Milwaukee, WI, USA). The scanning area covered the neck from the skull base to the thoracic inlet.

The scanning parameters were as follows: 120 kV, pitch 0.98, detector collimation 40 × 0.625 mm, rotation time 0.8 s, matrix 512 × 512, section thickness 0.625 mm, field

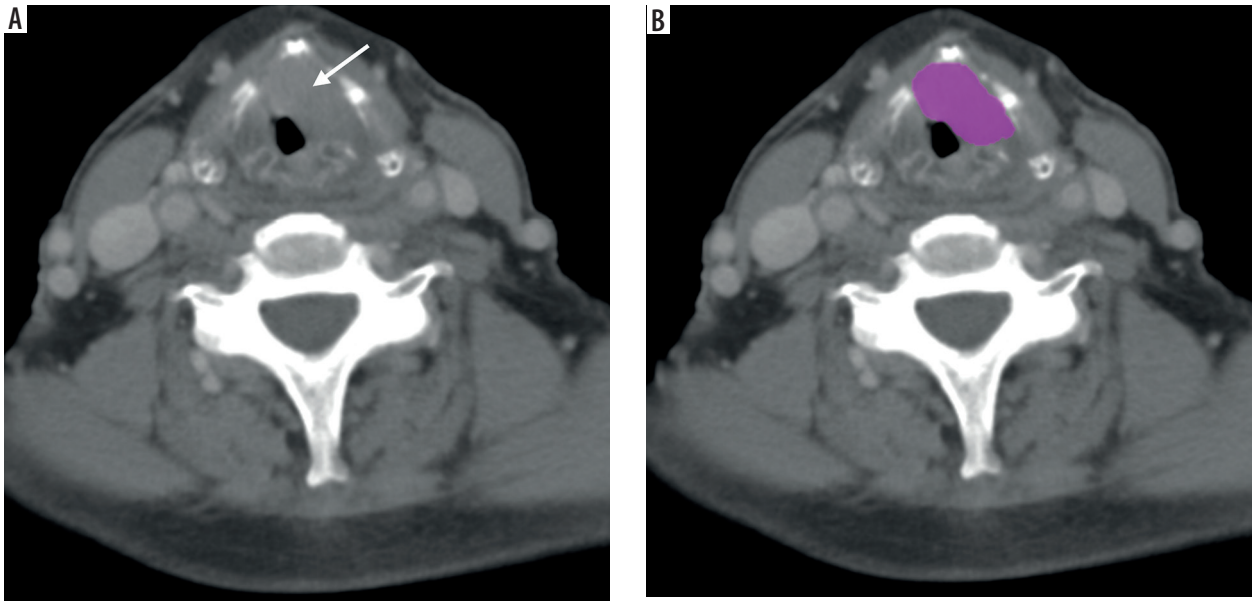

Figure 2. Tumor segmentation on axial computed tomography (CT). **A**) Axial contrast-enhanced CT image showing a mass invading the anterior commissure and the left vocal cord, extending into the paraglottic space (arrow). **B**) The region of interest (ROI) is delineated for texture analysis

of view, 220-250 mm, and automatic tube current modulation (8-320 mAs).

A non-ionic contrast agent (Ultravist 370 mg iodine/ml, Berlin, Germany) was administered using an automatic injector at 2-3 ml/s, followed by a 30-50 ml saline flush. Imaging was performed 40-50 s post-contrast in the venous phase.

CT-based texture analysis methodology

Texture analysis was performed using the freely available software LIFEx (Version 5.1, www.lifexsoft.org). Axial CT images were imported in Digital Imaging and Communications in Medicine (DICOM) format for radiomic feature extraction. The LIFEx software enabled synchronised visualisation of axial, coronal, and sagittal slices to facilitate precise tumour delineation [16]. All patient data were fully anonymised before image export and analysis to ensure confidentiality.

Two radiologists (with 17 and 8 years of experience in head and neck radiology) jointly performed the manual segmentation on axial contrast-enhanced CT images, blinded to histopathological outcomes. To minimise partial volume effects, regions of interest (ROIs) were manually delineated slightly within the tumour borders on each slice, with no ROI drawn on the first or last slices where the lesion was visible. Cystic areas were excluded from the delineation process.

For thyroid cartilage involvement, the ROI was drawn around the tumour region involving the thyroid cartilage. If the tumour extended across the cartilage to form an extralaryngeal mass, the extralaryngeal region was also included, while normal-appearing cartilage on the CT images was avoided (Figure 2).

The lesion extent was carefully determined by adjusting the window width and level and utilising multiplanar reconstruction to ensure accurate tumour measurement and consistency across different planes. For uniformity, the grey-level resolution was standardised to 128 levels (corresponding to a 7-bit depth). Intensity values were automatically rescaled based on the range defined by the mean ± 3 standard deviations (SD) of the ROI. Specifically, the lower and upper intensity limits were set to the mean minus 3 SD and the mean plus 3 SD, respectively, with any pixel values outside these bounds initially clipped to these thresholds. Moreover, to standardise voxel dimensions across the X, Y, and Z axes, the voxel sizes were adjusted to 0.5 mm in both the X and Y directions and 2.5 mm in the Z direction after computing the mean ± 3 SDs [17].

A total of 38 radiomic texture features were extracted. Specifically, 6 first-order histogram features (including parameters such as mean, standard deviation, skewness, and kurtosis, among others) were computed. In addition, second-order features were derived from multiple matrices: 7 features from the grey-level co-occurrence matrix (GLCM), 11 features from the gray-level run-length matrix (GLRLM), 3 features from the neighbourhood grey-level difference matrix (NGLDM), and 11 features from the grey-level zone-length matrix (GLZLM). Further details on texture analysis parameters can be found in Supplementary Table 1.

Statistical analyses were performed to evaluate the relationship between the extracted texture parameters and histopathological outcomes, including LNM, ENE, and TCI. Receiver operating characteristic (ROC) curve analysis was conducted to assess the diagnostic performance of significant texture features.

Histopathological analysis

All tumour specimens were fixed in 10% buffered formalin and embedded in paraffin according to standard procedures. Serial 5-µm thick sections were placed on positively charged slides and stained with haematoxylin and eosin (H&E) using a standardised protocol. Histopathological evaluation was performed by a pathologist with 18 years of experience, assessing LNM, ENE, LVI, perineural PNI, and TCI. Grading and staging were assigned according to the AJCC 8th edition criteria.

Statistical analysis

All statistical analyses were performed using SPSS version 26 (IBM Corp., Armonk, NY, USA). Continuous variables are presented as mean ± standard deviation, while categorical variables are expressed as frequencies and percentages. Normality was assessed using the Kolmogorov-Smirnov and Shapiro-Wilk tests. Group differences were evaluated with the Mann-Whitney *U* test. ROC curve analysis was conducted to determine the diagnostic performance of significant texture features. A p-value < 0.05 was considered statistically significant.

Results

The final study cohort comprised 32 patients, including 30 (93.75%) males and 2 (6.25%) females. The mean age was 62 ± 9.8 years. Demographic and clinicopathological characteristics of the study cohort are summarised in Table 1.

The distribution of all analysed texture parameters according to histopathological outcomes is presented in Supplementary Table 2.

Statistically significant texture feature distributions and their associated p-values are presented in Table 2. Among patients with LNM, 8 texture parameters reached statistical significance ($p < 0.05$). For ENE, 16 significant texture features were identified, and similarly, 16 texture parameters were significant for TCI. Notably, no significant texture parameters were found to differentiate LVI or PNI.

ROC curve analysis was performed on the texture features that significantly differentiated the histopathological outcomes, particularly for parameters with p-values ≤ 0.001. These features, which were significant in distinguishing LNM, ENE, and TCI, were further evaluated to determine the corresponding cut-off values, area under the curve (AUC), sensitivity, and specificity. These results are summarised in Table 3.

Table 1. Demographic and clinicopathological characteristics of the cohort

Characteristic	Subgroups	*N*	%
Age (years), mean ± SD (range)	62 ± 9.8 (25-75)		
Gender	Male	30	93.75
	Female	2	6.25
Surgery type	Partial laryngectomy	7	21.88
	Total laryngectomy	25	78.12
Tumour size (cm), mean ± SD (range)	2.89 ± 0.92 (25-75)		
Tumour subsite	Subglottic	2	6.25
	Transglottic/Glottic	22	68.75
	Supraglottic	8	25
T stage	T1-2	4	12.50
	T3	13	40.62
	T4	15	46.88
N stage	N0	14	43.75
	N1	6	18.75
	N2	5	15.62
	N3	7	21.88
Lymph node metastasis (LNM)	Present	14	43.75
	Absent	18	56.25
Extranodal extension (ENE)	Present	7	21.88
	Absent	25	78.12
Lymphovascular invasion (LVI)	Present	9	28.12
	Absent	23	71.88
Perineural invasion (PNI)	Present	7	21.88
	Absent	25	78.12
Thyroid cartilage invasion (TCI)	Present	18	56.25
	Absent	14	43.75

Table 2. Statistically significant texture feature values by histopathological outcomes in laryngeal cancer ($p < 0.05$)

Histopathological outcome	Texture feature	Feature class	*n*	Present (mean ± SD)	*n*	Absent (mean ± SD)	*p*-value*
LNM	Contrast	GLCM	14	376.14 ± 171.04	18	509.94 ± 143.12	0.045
LNM	Correlation	GLCM	14	0.57 ± 0.19	18	0.43 ± 0.15	0.041
LNM	Dissimilarity	GLCM	14	14.78 ± 3.79	18	17.58 ± 2.82	0.037
LNM	SRE	GLRLM	14	0.98 ± 0.01	18	0.99 ± 0.00	0.045
LNM	HGRE	GLRLM	14	4606.43 ± 12.16	18	4616.67 ± 4.85	0.008
LNM	LRHGE	GLRLM	14	4964.29 ± 139.32	18	4874.44 ± 62.33	0.049
LNM	HGZE	GLZLM	14	4617.14 ± 24.00	18	4645.00 ± 25.50	0.000
LNM	LZHGE	GLZLM	14	14718.57 ± 8837.49	18	10002.78 ± 1918.30	0.049
ENE	Energy	GLCM	7	0.00 ± 0.00	25	0.00 ± 0.00	0.026
ENE	Contrast	GLCM	7	279.71 ± 146.00	25	499.48 ± 141.05	0.003
ENE	Correlation	GLCM	7	0.68 ± 0.16	25	0.44 ± 0.15	0.002
ENE	Entropy-log10	GLCM	7	3.46 ± 0.17	25	3.59 ± 0.18	0.043
ENE	Entropy-log2	GLCM	7	11.49 ± 0.56	25	11.92 ± 0.60	0.034
ENE	Dissimilarity	GLCM	7	12.68 ± 3.53	25	17.38 ± 2.80	0.003
ENE	SRE	GLRLM	7	0.98 ± 0.01	25	0.99 ± 0.00	0.015
ENE	LRE	GLRLM	7	1.09 ± 0.03	25	1.06 ± 0.02	0.018
ENE	HGRE	GLRLM	7	4604.29 ± 11.34	25	4614.40 ± 8.70	0.026
ENE	LRHGE	GLRLM	7	5014.29 ± 144.90	25	4885.60 ± 83.02	0.010
ENE	RP	GLRLM	7	0.97 ± 0.01	25	0.98 ± 0.01	0.013
ENE	SZE	GLZLM	7	0.79 ± 0.06	25	0.85 ± 0.03	0.020
ENE	LZE	GLZLM	7	3.30 ± 1.34	25	2.31 ± 0.76	0.015
ENE	HGZE	GLZLM	7	4602.86 ± 24.30	25	4641.20 ± 23.33	0.001
ENE	LZHGE	GLZLM	7	15820.00 ± 7367.73	25	11014.80 ± 5777.21	0.011
ENE	ZP	GLZLM	7	0.70 ± 0.08	25	0.78 ± 0.05	0.010
TCI	Energy	GLCM	18	0.00 ± 0.00	14	0.00 ± 0.00	0.030
TCI	Contrast	GLCM	18	532.44 ± 125.21	14	347.21 ± 159.99	0.001
TCI	Correlation	GLCM	18	0.40 ± 0.12	14	0.60 ± 0.17	0.001
TCI	Entropy-log10	GLCM	18	3.62 ± 0.12	14	3.47 ± 0.22	0.030
TCI	Dissimilarity	GLCM	18	18.05 ± 2.40	14	14.17 ± 3.59	0.001
TCI	SRE	GLRLM	18	0.98 ± 0.00	14	0.98 ± 0.01	0.011
TCI	LRE	GLRLM	18	1.05 ± 0.01	14	1.07 ± 0.02	0.034
TCI	LRHGE	GLRLM	18	4875.56 ± 73.98	14	4962.85 ± 132.68	0.018
TCI	RP	GLRLM	18	0.98 ± 0.00	14	0.97 ± 0.00	0.016
TCI	Contrast	NGLDM	18	0.72 ± 0.10	14	0.59 ± 0.20	0.009
TCI	SZE	GLZLM	18	0.85 ± 0.03	14	0.81 ± 0.05	0.011
TCI	LZE	GLZLM	18	2.20 ± 0.56	14	2.93 ± 1.25	0.020
TCI	LGZE	GLZLM	18	0.00 ± 0.00	14	0.00 ± 0.00	0.000
TCI	SZLGE	GLZLM	18	0.00 ± 0.00	14	0.00 ± 0.00	0.000
TCI	LZHGE	GLZLM	18	10112.22 ± 2625.37	14	14577.85 ± 8677.05	0.025
TCI	ZP	GLZLM	18	0.78 ± 0.04	14	0.73 ± 0.07	0.016

*p-values are based on the Mann-Whitney U test.

LNM – lymph node metastasis, ENE – extranodal extension, TCI – thyroid cartilage invasion, GLCM – grey-level co-occurrence matrix, GLRLM – gray-level run length matrix, GLZLM – gray-level zone length matrix, NGLDM – neighbourhood grey-level difference matrix, SRE – short run emphasis, LRE – long run emphasis, HGRE – high grey-level run emphasis, LRHGE – long run high grey-level emphasis, SZE – short zone emphasis, LZE – long zone emphasis, HGZE – high grey-level zone emphasis, LZHGE – long zone high grey-level emphasis, LGZE – low grey-level zone emphasis, SZLGE – short zone low grey-level emphasis, RP – run percentage, ZP – zone percentage

Table 3. Cut-off values and diagnostic accuracy of texture features for predicting histopathological outcomes in laryngeal cancer

Histopathological outcome	Texture feature	Feature class	Area under the curve	95% Confidence interval	Cutoff value	Sensitivity (%)	Specificity (%)	*p*
LNM	HGZE	GLZLM	0.847	0.708-0.986	≤ 4635	71	84	0.001
ENE	HGZE	GLZLM	0.891	0.764-1.000	≤ 4625	85	84	0.002
TCI	Contrast	GLCM	0.829	0.689-0.970	≥ 437	88	65	0.002
TCI	Dissimilarity	GLCM	0.829	0.688-0.971	≥ 16.3	88	65	0.002
TCI	LGZE	GLZLM	0.903	0.800-1.000	≥ 0.0015	88	79	< 0.001
TCI	SZLGE	GLZLM	0.964	0.909-1.000	≥ 0.00118	88	93	< 0.001
TCI	Correlation	GLCM	0.835	0.697-0.973	≤ 0.51	88	65	0.001

LNM – lymph node metastasis, ENE – extranodal extension, TCI – thyroid cartilage invasion, GLZLM – grey level zone length matrix, GLCM – grey level co-occurrence matrix, HGZE – high grey level zone emphasis, LGZE – low grey level zone emphasis, SZLGE – small zone low grey level emphasis, *p* – probability value

For LNM, the texture feature GLZLM_High Gray-Level Zone Emphasis (HGZE) was significant; a cut-off value of ≤ 4635 yielded an AUC of 0.847 (95% CI, 0.708-0.986), with a sensitivity of 71% and a specificity of 84% ($p = 0.001$).

For ENE, GLZLM_HGZE was also significant, with a cut-off value of ≤ 4625 resulting in a sensitivity of 85% and a specificity of 84% ($p = 0.002$).

For TCI, among the significant texture features, both GLZLM_Low Gray-Level Zone Emphasis (LGZE) and GLZLM_Short Zone Low Gray-Level Emphasis (SZLGE) demonstrated robust performance. Specifically, GLZLM_LGZE showed a cut-off value of ≥ 0.0015 with a sensitivity of 88% and a specificity of 79% ($p < 0.001$), while GLZLM_SZLGE exhibited a cut-off value of ≥ 0.00118, yielding an AUC of 0.964 (95% CI, 0.909-1.000), a sensitivity of 88%, and a specificity of 93% ($p < 0.001$).

Discussion

This study investigated the potential of CT-based radiomic analysis for predicting adverse histopathological outcomes in laryngeal cancer, focusing on LNM, ENE, and TCI. Significant differences in texture features – including GLZLM_HGZE for LNM and ENE, and GLZLM_LGZE and GLZLM_SZLGE for TCI – highlight the diagnostic value of radiomics as a non-invasive tool. Our findings demonstrated robust AUC values and favourable sensitivity/specificity, supporting the role of radiomics as a potential biomarker.

Preoperative identification of LNM and ENE is essential in HNSCC, as both are poor prognostic factors that often require treatment escalation, including the addition of chemotherapy to adjuvant radiotherapy. Early detection can enhance risk stratification and treatment planning, potentially reducing the need for extensive surgery or overtreatment [18,19]. In our study, GLZLM_HGZE was significantly associated with both ENE (AUC: 0.891; sensitivity: 85%, specificity: 84%) and LNM (AUC: 0.847; sensitivity: 71%, specificity: 84%), underscoring its value as a non-invasive imaging biomarker for assessing nodal and perinodal tumour spread. As a texture metric emphasising high-intensity homogeneous regions, GLZLM_HGZE probably reflects areas of dense tumour cellularity or desmoplastic stromal response – histopathological characteristics frequently linked to aggressive metastatic behaviour in head and neck cancers [8,20]. These biological correlates may explain the observed predictive capacity of this feature in evaluating metastatic potential.

Although studies on texture-based ENE and LNM prediction are limited in LSCC, radiomic models have shown high diagnostic accuracy in the broader HNSCC group [21-23]. For instance, machine learning-assisted texture analysis using dual-energy CT (DECT) successfully differentiated metastatic lymph nodes from benign conditions with 80-95% accuracy [24]. Another study extracted 99 radiomic features from 630 lymph nodes and applied random forest and deep neural networks, achieving an AUC of 0.91 for ENE and LNM detection [25]. These results support the role of radiomic analysis in improving nodal staging, emphasising the need for further multi-centre validation to enhance its clinical applicability.

A multi-institutional study by Kann *et al.* [26] validated a deep learning model for ENE detection in patients with HNSCC, achieving AUCs of 0.84-0.90, outperforming expert radiologists. Their findings highlight the clinical potential of AI-driven radiomics, underscoring the need for large-scale, multi-centre studies to further establish radiomic and AI-based models in ENE prediction and treatment planning.

In our study, no significant texture features were identified for predicting LVI and PNI, suggesting limited radiomic detectability. One possible reason is the exclusion of peritumoral texture features, which have shown promise in LVI prediction. Xu *et al.* [27] developed a CT-based radiomics model for LVI prediction in hypopharyngeal squamous cell carcinoma (HSCC), incorporating intratumoral and peritumoral features from 166 patients. Their model achieved high predictive performance (AUC 0.94-0.96), with peritumoral features (1 mm beyond tumour margins) showing the strongest association with LVI. These findings highlight the importance of peritumoral texture analysis, which was not included in our study and may explain the lack of significant predictive features.

Similarly, Mukherjee *et al.* [28] investigated CT-based radiomics for LVI and PNI prediction in HNSCC, reporting moderate performance (AUCs: 0.69/0.64 for LVI/PNI in the training cohort; 0.65/0.70 in the test cohort). This suggests that radiomic analysis reflects tumour heterogeneity, although with limited predictive accuracy.

Further supporting radiomics in PNI prediction, Li *et al.* [29] developed a CT-based delta radiomics nomogram for PNI assessment in HSCC, combining tumour thickness and radiomic features. Their model outperformed clinical models (AUCs: 0.79/0.78 in training/test cohorts), demonstrating radiomics' potential for non-invasive PNI detection, although further validation is needed.

Accurate preoperative identification of cartilage invasion in LSCC is crucial for staging and treatment planning, particularly in distinguishing total laryngectomy cases from organ-preserving candidates. Studies comparing CT, MRI, and DECT have shown significant differences in diagnostic performance. A meta-analysis reported that MRI had higher sensitivity (90% vs. 66%) but lower specificity (81% vs. 88%) than CT, suggesting more false positives due to inflammatory changes [30]. Similarly, DECT demonstrated superior specificity (100% vs. 64%) for thyroid cartilage invasion, with comparable sensitivity (89% vs. 100%) [31]. Given these variations, integrating radiomics and AI-based analysis may further improve diagnostic accuracy and clinical decision-making.

Guo *et al.* [14] demonstrated that CT-based radiomics models (LR and LR-SVMSMOTE) significantly outperformed radiologists in TCI prediction (AUCs: 0.876 and 0.905 vs. 0.721), highlighting the value of machine learning-driven feature selection. In line with these findings, our study identified GLCM_Contrast, GLCM_Dissimilarity, GLZLM_LGZE, GLZLM_SZLGE, and GLCM_Correlation as significant predictors of TCI, with robust AUC values and well-defined cut-off thresholds. These second-order GLCM-derived features quantify local intensity variation and grey-level spatial relationships, with higher values generally reflecting disrupted tissue architecture, increased intratumoural heterogeneity, and transition zones between malignant and reactive components – hallmarks of invasive tumour growth into adjacent structures such as cartilage.

GLZLM_LGZE and GLZLM_SZLGE, both strongly associated with thyroid cartilage invasion, emphasise low-intensity zones of varying sizes. While LGZE captures broader hypodense areas potentially indicative of stromal degradation or acellular necrosis (AUC: 0.903), SZLGE highlights smaller homogeneous regions that may reflect focal necrosis, disorganised stroma, or poorly differentiated tumour nests (AUC: 0.964). Together, these features characterise distinct aspects of aggressive tumour biology and may serve as reliable imaging biomarkers for local invasive behaviour[7,32].

While mechanistic validation remains limited, these findings reinforce the potential of CT-based texture analysis as a non-invasive tool for assessing tumour aggressiveness and microstructural complexity in head and neck squamous cell carcinoma, particularly in predicting TCI [9,33]. Further validation using multimodal imaging and AI-driven approaches is warranted to enhance clinical applicability.

This study has several limitations. First, the relatively small sample size limited the ability to develop a machine learning-based predictive model. Instead, we focused on evaluating the diagnostic performance of selected radiomic parameters through ROC analysis, assessing their clinical applicability in predicting LNM, ENE, and TCI. Second, the study was conducted retrospectively at a single institution, which may limit the generalisability of the findings. A larger, multi-centre dataset would improve model robustness and external validation. Third, interobserver agreement for manual ROI segmentation was not quantitatively assessed (e.g., using ICC or Dice coefficient), which may introduce variability in feature extraction; however, segmentation was performed by experienced radiologists following standardised criteria. Fourth, peritumoral texture features were not included, which have shown predictive value in previous studies. Future research incorporating both intratumoral and peritumoral radiomic features may enhance diagnostic accuracy. Lastly, we used CT-derived radiomics, while MRI-based radiomics may provide complementary insights due to its superior soft-tissue contrast. Further studies comparing CT- and MRI-based radiomic models could refine imaging-based prediction strategies for laryngeal cancer management. Future research should focus on developing machine learning-based models with larger, balanced datasets to improve predictive accuracy. Despite these limitations, our study demonstrated that the identified radiomic parameters, with well-defined cut-off values, hold clinical relevance as non-invasive biomarkers for LNM, ENE, and TCI assessment.

Conclusions

CT-based texture analysis demonstrates potential as a non-invasive tool for predicting key histopathological features in LSCC, particularly LNM, ENE, and TCI. Significant radiomic parameters showed high diagnostic accuracy, supporting their role in preoperative risk stratification. Further validation in larger, multi-centre studies is necessary to enhance clinical applicability and integration into routine oncologic imaging.

Disclosures

1. Institutional review board statement: Ethics Committee Approval – Decision No. 2024/247, 08.01.2025.
2. Assistance with the article: AI assistance was used for language editing and grammar correction.
3. Financial support and sponsorship: None.
4. Conflicts of interest: None.

References

1. Huang J, Chan SC, Ko S, Lok V, Zhang L, Lin X, et al. Updated disease distributions, risk factors, and trends of laryngeal cancer: a global analysis of cancer registries. Int J Surg 2024; 110: 810-819.
2. Bradford CR, Ferlito A, Devaney KO, Mäkitie AA, Rinaldo A. Prognostic factors in laryngeal squamous cell carcinoma. Laryngoscope Investig Otolaryngol 2020; 5: 74-81.
3. Geisler SA, Olshan AF, Weissler MC, Cai J, Funkhouser WK, Smith J, et al. P16 and P53 Protein expression as prognostic indicators of survival and disease recurrence from head and neck cancer. Clin Cancer Res 2002; 8: 3445-3453.
4. Shin H Il, Bang JI, Kim GJ, Sun D Il, Kim SY. Perineural invasion predicts local recurrence and poor survival in laryngeal cancer. J Clin Med 2023; 12: 449.
5. Zhu X, Duan F, Zhu Y, Shi X, Sun S, Cheng Y, et al. Perineural invasion as a prognostic factor in laryngeal squamous cell cancer: a matched-pair survival analysis. Cancer Invest 2021; 39: 734-740.
6. Montenegro C, Paderno A, Ravanelli M, Pessina C, Nassih FE, Lancini D, et al. Thyroid cartilage infiltration in advanced laryngeal cancer: prognostic implications and predictive modelling. Acta Otorhinolaryngol Ital 2024; 44: 176-182.
7. Meyer HJ, Hamerla G, Höhn AK, Surov A. CT texture analysis-correlations with histopathology parameters in head and neck squamous cell carcinomas. Front Oncol 2019; 9: 1-8.
8. de Oliveira LAP, Lopes DLG, Gomes JPP, da Silveira RV, Nozaki DVA, Santos LF, et al. Enhanced diagnostic precision: assessing tumor differentiation in head and neck squamous cell carcinoma using multi-slice spiral CT texture analysis. J Clin Med 2024; 13: 1-9.
9. Haider SP, Burtness B, Yarbrough WG, Payabvash S. Applications of radiomics in precision diagnosis, prognostication and treatment planning of head and neck squamous cell carcinomas. Cancers Head Neck 2020; 5: 1-19.
10. Fujima N, Kamagata K, Ueda D, Fujita S, Fushimi Y, Yanagawa M, et al. Current state of artificial intelligence in clinical applications for head and neck MR imaging. Magn Reson Med Sci 2023; 22: 401-414.
11. Zhang H, Graham CM, Elci O, Griswold ME, Zhang X, Khan MA, et al. Locally advanced squamous cell carcinoma of the head and neck: CT texture and histogram analysis allow independent prediction of overall survival in patients treated with induction chemotherapy. Radiology 2013; 269: 801-809.
12. Doillon M, Durot C, Pluchart C, Marcus C, Djelouah M, Carsin-Vu A. Response to induction therapy in pediatric Hodgkin's lymphoma: performance of first-order texture parameters of CT images. J Belgian Soc Radiol 2022; 106: 1-7.
13. Altay C, Başara Akın I, Özgül AH, Adıyaman SC, Yener AS, Seçil M. Machine learning analysis of adrenal lesions: preliminary study evaluating texture analysis in the differentiation of adrenal lesions. Diagnostic Interv Radiol 2023; 29: 234-243.
14. Guo R, Guo J, Zhang L, Qu X, Dai S, Peng R, et al. CT-based radiomics features in the prediction of thyroid cartilage invasion from laryngeal and hypopharyngeal squamous cell carcinoma. Cancer Imaging 2020; 20: 81.
15. Rajgor AD, Kui C, Mcqueen A, Cowley J, Gillespie C, Mill A, et al. Computed tomography-based radiomic markers are independent prognosticators of survival in advanced laryngeal cancer: a pilot study. J Laryngol Otol 2024; 138: 685-691.
16. Nioche C, Orlhac F, Boughdad S, Reuze S, Goya-Outi J, Robert C, et al. Lifex: A freeware for radiomic feature calculation in multimodality imaging to accelerate advances in the characterization of tumor heterogeneity. Cancer Res 2018; 78: 4786-4789.
17. Rizzo S, Botta F, Raimondi S, Origgi D, Fanciullo C, Morganti AG, et al. Radiomics: the facts and the challenges of image analysis. Eur Radiol Exp 2018; 2: 36.
18. Xu B, Saliba M, Alzumaili B, Alghamdi M, Lee N, Riaz N, et al. Prognostic impact of extranodal extension (ENE) in surgically managed treatment-naive HPV-positive oropharyngeal squamous cell carcinoma with nodal metastasis. Mod Pathol 2022; 35: 1578-1586.
19. Chang CW, Wang C, Lu CJ, Wang CW, Wu CT, Wang CP, et al. Incidence and prognostic significance of extranodal extension in isolated nodal recurrence of oral squamous cell carcinoma. Radiother Oncol 2022; 167: 81-88.
20. Tortora M, Gemini L, Scaravilli A, Ugga L, Ponsiglione A, Stanzione A, et al. Radiomics applications in head and neck tumor imaging: a narrative review. Cancers 2023; 15: 1174.
21. Huang TT, Lin YC, Yen CH, Lan J, Yu CC, Lin WC, et al. Prediction of extranodal extension in head and neck squamous cell carcinoma by CT images using an evolutionary learning model. Cancer Imaging 2023; 23: 1-11.
22. Romeo V, Cuocolo R, Ricciardi C, Ugga L, Cocozza S, Verde F, et al. Prediction of Tumor Grade and Nodal Status in Oropharyngeal and Oral Cavity Squamous-cell Carcinoma Using a Radiomic Approach. Anticancer Res 2020; 40: 271-280.
23. Ho TY, Chao CH, Chin SC, Ng SH, Kang CJ, Tsang NM. Classifying neck lymph nodes of head and neck squamous cell carcinoma in MRI images with radiomic features. J Digit Imaging 2020; 33: 613-618.
24. Seidler M, Forghani B, Reinhold C, Pérez-Lara A, Romero-Sanchez G, Muthukrishnan N, et al. Dual-energy CT texture analysis with machine learning for the evaluation and characterization of cervical lymphadenopathy. Comput Struct Biotechnol J 2019; 17: 1009-1015.
25. Kann BH, Aneja S, Loganadane GV, Kelly JR, Smith SM, Decker RH, et al. Pretreatment identification of head and neck cancer nodal metastasis and extranodal extension using deep learning neural networks. Sci Rep 2018; 8: 14036.
26. Kann BH, Hicks DF, Payabvash S, Mahajan A, Du J, Gupta V, et al. Multi-institutional validation of deep learning for pretreatment identification of extranodal extension in head and neck squamous cell carcinoma. J Clin Oncol 2020; 38: 1304-1311.
27. Xu C, Ju Y, Liu Z, Li C, Cao S, Xia T, et al. Radiomics model based on contrast-enhanced CT intratumoral and peritumoral features for predicting lymphovascular invasion in hypopharyngeal squamous cell carcinoma. Acad Radiol 2024; 2: 1-12.
28. Mukherjee P, Cintra M, Huang C, Zhou M, Zhu S, Colevas AD, et al. CT-based radiomic signatures for predicting histopathologic

features in head and neck squamous cell carcinoma. Radiol Imaging Cancer 2020; 2: e190039. DOI: 10.1148/rycan.2020190039.
29. Li J, Jiang N, Zhang J, Sun W, Wang Z, Sun L, et al. Computed tomography-based absolute delta radiomics nomogram for predicting perineural invasion in hypopharyngeal squamous cell carcinoma. Eur J Radiol 2025; 183: 111912.
30. Cho SJ, Lee JH, Suh CH, Kim JY, Kim D, Lee J Bin, et al. Comparison of diagnostic performance between CT and MRI for detection of cartilage invasion for primary tumor staging in patients with laryngo-hypopharyngeal cancer: a systematic review and meta-analysis. Eur Radiol 2020; 30: 3803-3812.
31. Kuno H, Sakamaki K, Fujii S, Sekiya K, Otani K, Hayashi R, et al. Comparison of MR imaging and dual-energy ct for the evaluation of cartilage invasion by laryngeal and hypopharyngeal squamous cell carcinoma. Am J Neuroradiol 2018; 39: 524-531.
32. Avanzo M, Wei L, Stancanello J, Vallières M, Rao A, Morin O, et al. Machine and deep learning methods for radiomics. Med Phys 2020; 47: e185-e202.
33. Wang F, Zhang B, Wu X, Liu L, Fang J, Chen Q, et al. Radiomic nomogram improves preoperative T category accuracy in locally advanced laryngeal carcinoma. Front Oncol 2019; 9: 1064.